LAWRENCE
LIVERMORE
NATIONAL
LABORATORY

Combined near- and far-field high-energy diffraction microscopy dataset for Ti-7Al tensile specimen elastically loaded in situ

T. J. Turner, P. A. Shade, J. V. Bernier, S. -F. Li, J. C. Schuren, J. Lind, U. Lienert, P. Kenesei, R. M. Suter, B. Blank, J. Almer

September 17, 2017

Disclaimer

This document was prepared as an account of work sponsored by an agency of the United States government. Neither the United States government nor Lawrence Livermore National Security, LLC, nor any of their employees makes any warranty, expressed or implied, or assumes any legal liability or responsibility for the accuracy, completeness, or usefulness of any information, apparatus, product, or process disclosed, or represents that its use would not infringe privately owned rights. Reference herein to any specific commercial product, process, or service by trade name, trademark, manufacturer, or otherwise does not necessarily constitute or imply its endorsement, recommendation, or favoring by the United States government or Lawrence Livermore National Security, LLC. The views and opinions of authors expressed herein do not necessarily state or reflect those of the United States government or Lawrence Livermore National Security, LLC, and shall not be used for advertising or product endorsement purposes.

DATA DESCRIPTOR   **Open Access**

CrossMark

Combined near- and far-field high-energy diffraction microscopy dataset for Ti-7Al tensile specimen elastically loaded in situ

Todd J. Turner[1*], Paul A. Shade[1], Joel V. Bernier[2], Shiu Fai Li[2], Jay C. Schuren[1], Jonathan Lind[2,3], Ulrich Lienert[4], Peter Kenesei[5], Robert M. Suter[3], Basil Blank[6] and Jonathan Almer[5]

* Correspondence:
Todd.Turner.5@us.af.mil
[1]Materials and Manufacturing Directorate, Air Force Research Laboratory, 2230 10th Street, Wright-Patterson AFB, OH 45433, USA
Full list of author information is available at the end of the article

Abstract

High-energy diffraction microscopy (HEDM) constitutes a suite of combined X-ray characterization methods, which hold the unique advantage of illuminating the microstructure and micromechanical state of a material during concurrent in situ mechanical deformation. The data generated from HEDM experiments provides a heretofore unrealized opportunity to validate meso-scale modeling techniques, such as crystal plasticity finite element modeling (CPFEM), by explicitly testing the accuracy of these models at the length scales where the models predict their response. Combining HEDM methods with in situ loading under known and controlled boundary conditions represents a significant challenge, inspiring the recent development of a new high-precision rotation and axial motion system for simultaneously rotating and axially loading a sample. In this paper, we describe the initial HEDM dataset collected using this hardware on an alpha-titanium alloy (Ti-7Al) under in situ tensile deformation at the Advanced Photon Source, Argonne National Laboratory. We present both near-field HEDM data that maps out the grain morphology and intragranular crystallographic orientations and far-field HEDM data that provides the grain centroid, grain average crystallographic orientation, and grain average elastic strain tensor for each grain. Finally, we provide a finite element mesh that can be utilized to simulate deformation in the volume of this Ti-7Al specimen. The dataset supporting this article is available in the National Institute of Standards and Technology (NIST) repository (http://hdl.handle.net/11256/599).

Keywords: High-energy diffraction microscopy (HEDM), X-ray diffraction, Far-field diffraction, Near-field diffraction, Three-dimensional microstructure, Crystal plasticity finite element modeling (CPFEM)

Data description

Introduction

High-energy diffraction microscopy (HEDM) is a suite of experimental techniques that utilizes high-energy monochromatic synchrotron radiation to non-destructively interrogate the microstructure and micromechanical state of a material during deformation [1–3]. This offers a powerful tool to characterize the internal structure and mechanical behavior of deformable solids, which can be used to instantiate, and then later validate, micro- and meso-scale models such as crystal plasticity finite element modeling

Springer

Turner *et al. Integrating Materials and Manufacturing Innovation*

Page 2 of 9

(CPFEM) [4–6]. The dataset presented in this paper represents concurrently collected near-field HEDM (nf-HEDM) [7–9] and far-field HEDM (ff-HEDM) measurements [10–13]; a first analysis of these data is contained in [14]. The nf-HEDM technique utilizes an area detector placed approximately 5 mm from the specimen and measures the grain morphology and local crystallographic orientations within and between grains, while the ff-HEDM technique measures the centroid and the average elastic strain tensor and crystallographic orientation in each individual grain. These data are co-registered into a single HEDM dataset that tracks the deformation of a polycrystalline material during in situ mechanical loading.
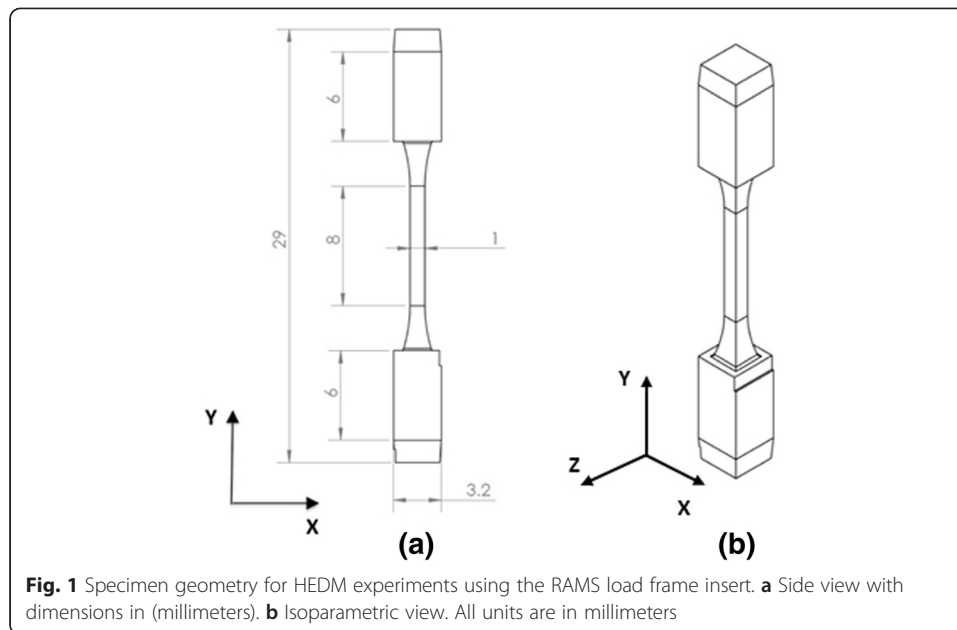
Material

The titanium alloy utilized in this experiment (Ti-7Al) was a single-phase (α, hexagonal close-packed crystal structure) material. It was initially cast as a 75-mm ingot, hot isostatic pressed before being extruded into a 30-mm^2 bar. It was then uni-directionally rolled at 955 °C to a final thickness of 7.5 mm. The material was then recrystallized at 955 °C for 24 h and furnace cooled. This produced a single-phase material with a grain size of approximately 100 μm [1, 14]. The tensile specimen was fabricated with the tensile axis transverse to the rolling and normal directions. The material has significant elastic and plastic anisotropy [15–18], making it an ideal material to study with HEDM in order to examine the heterogeneity that develops even within the initial elastic portion of loading.

Experimental methods

The specific dataset presented here was collected in an HEDM experiment that was conducted at the 1-ID-E beamline of the Advanced Photon Source (APS) at Argonne National Laboratory (ANL). The experimental methods are generally described in Schuren et al. [1], and the specific in situ loading equipment developed for this, as well as the subsequent experiments, is detailed in Shade et al. [14]. Specifically, we utilized a rotational and axial motion system (RAMS) [14] to concurrently rotate the tensile specimen seen in Fig. 1, while applying an axial load. The RAMS is an insert held inside an MTS 858 load frame, whereby load is transferred to the sample through the load frame and RAMS device, while the RAMS provides simultaneous and independent rotation of the specimen during the experiment. As indicated in Fig. 1, the specimen had an initial 8-mm gage length, with a cross section of approximately 1×1 mm.

Before the specimen was loaded, ff-HEDM data were collected in a volume that spanned 600 μm along the gage length and included the entire 1×1 mm gage cross section. A 600-μm tall "box" X-ray beam was used to define the measurement volume for this dataset. The ff-HEDM measurements took approximately 12 min in order to fully rotate the specimen in 0.25° rotation intervals over a rotation range of 360°. Subsequent analysis of the diffraction patterns utilizing the HEXRD code [13] provided a characterization of the initial grain centroid location, as well as the full average elastic strain tensor in each grain before deformation[1] with a resolution of $\sim 1 \times 10^{-4}$. Next, we collected nf-HEDM data over a 200-μm long volume in the middle of the larger ff-HEDM volume, utilizing a 2-μm tall line-focused X-ray beam. These measurements took approximately 24 h to complete. We analyzed the nf-HEDM diffraction data

Turner *et al. Integrating Materials and Manufacturing Innovation*

Page 3 of 9

Fig. 1 Specimen geometry for HEDM experiments using the RAMS load frame insert. **a** Side view with dimensions in (millimeters). **b** Isoparametric view. All units are in millimeters
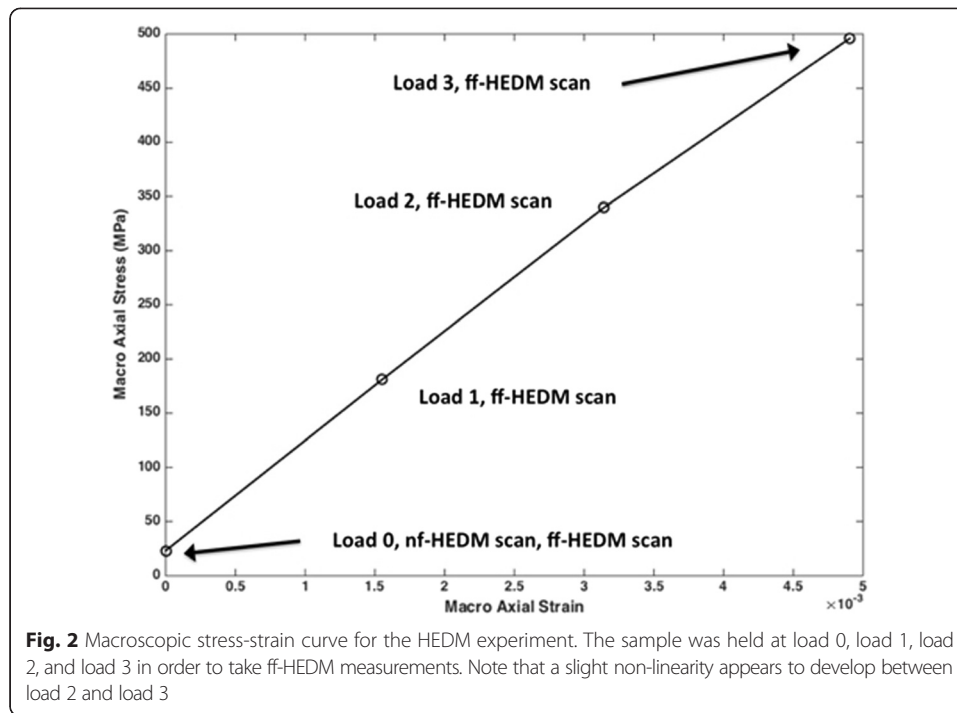
with the IceNine data reduction code [9] to characterize the 3D grain morphology and intragranular orientation distribution, with a spatial resolution of ~2 μm and an accuracy of ~0.1^{0} in crystallographic orientation. During these measurements, a small axial load (23 MPa) existed on the specimen as a result of the specimen loading procedure, where a slight axial translation was unavoidable while tightening the grips that held the specimen during testing. This initial unloaded state will hereafter be referred to as *load 0*.

After the initial HEDM measurements at load 0, we loaded along the *y*-axis of the specimen to three additional levels (*load 1* (180.88 MPa), *load 2* (339.81 MPa), *Load 3* (495.90 MPa)), each below the macroscopic yield point (Fig. 2), where we conducted ff-HEDM measurements at each load level. The specimen was initially overloaded past each of these desired axial load levels and then unloaded approximately 10 % to minimize any change in material state during the ff-HEDM measurements due to stress relaxation [19]. From Fig. 2, it becomes apparent that the loading curve deviates from linearity between load 2 and load 3, which is likely an indication of the onset of plasticity. The strain levels were measured by a two-point digital image correlation on the surface of the specimen, specifically by measuring the distance between two gold fiducial markers placed on the surface that also serve as reference features for alignment [20]. In this manner, the initial strain at load 0 is assumed to be zero, despite the 23-MPa axial load, as no DIC measurement was made prior to clamping the specimen in the grips.

Dataset description

The dataset supporting the results of this article is available in the National Institute of Standards and Technology (NIST) repository (http://hdl.handle.net/11256/599), containing a single HDF5 file (https://www.hdfgroup.org), a format designed to store large

Turner *et al. Integrating Materials and Manufacturing Innovation*

Page 4 of 9

Fig. 2 Macroscopic stress-strain curve for the HEDM experiment. The sample was held at load 0, load 1, load 2, and load 3 in order to take ff-HEDM measurements. Note that a slight non-linearity appears to develop between load 2 and load 3

datasets whereby a portion of the file may be extracted for analysis without having to load the entire dataset into memory. This provides a highly efficient file format for manipulating large data and can be conveniently viewed with HDF5Viewer (https://www.hdfgroup.org/products/java/hdfview/).

In the HDF5 file, the folder titled *Sample* contains the *Macro Strain* and the *Macro Stress* data fields. These fields provide the stress-strain data plotted in Fig. 2, representing the points in the test (load 0, load 1, load 2, and load 3) where the specimen was held under load to capture the ff-HEDM measurements.

The ff-HEDM data is also contained within the HDF5 file, including *Confidence Index*, *Elastic Constants*, *Grain ID*, and *nFFgrains*. These fields are found in the main *Farfield* folder in the file and represent data that are applicable to each load step. The nFFgrains field is a scalar number representing the number of grains in the ff-HEDM diffraction volume (605). Confidence Index is a similar metric as in the nf-HEDM data, containing a value between 0.0 and 1.0 representing the fit of the diffraction data to a certainty of the underlying datapoint evaluated by HEXRD in the initial analysis. Elastic Constants is a field with five single-crystal elastic constants (C_{11}, C_{12}, C_{13}, C_{33}, C_{44}), used to convert the elastic strain in the ff-HEDM data into stress [21–23]. Grain ID is a scalar value that uniquely identifies each grain in both ff-HEDM and nf-HEDM datasets.

In addition, each load step (load 0, load 1, load 2, and load 3) has a folder inside the Farfield folder that contains ff-HEDM data specific to that load level. Each of these folders contains the following variables: *Centroid*, *Grain Mean Strain*, *Grain Mean Stress*, and *Quaternions*. The Centroid field contains the Cartesian location of each grain centroid. Grain Mean Strain is the full 3D elastic strain tensor determined from HEXRD, written in

Turner *et al. Integrating Materials and Manufacturing Innovation*

Page 5 of 9

vector notation (ε_{11}, ε_{22}, ε_{33}, ε_{23}, ε_{13}, ε_{12}) (https://github.com/FrankieLi/IceNine). Grain Mean Stress is determined by using the *Elastic Constants* in conjunction with the *Elastic Strains*. It is also written in vector notation (σ_{11}, σ_{22}, σ_{33}, σ_{23}, σ_{13}, σ_{12}). Finally, the Quaternions field contains the crystallographic orientation of each grain in the ff-HEDM volume written in the quaternion orientation parameterization [24].

The file also contains the nf-HEDM data collected at load 0 to measure the morphology and intragranular orientation distribution of grains in the specimen. This data was reduced from the raw diffraction data through the use of the IceNine analysis software. These data contain multiple points within each grain, for a total of 3,388,294 data points. The nf-HEDM data were aligned with the initial ff-HEDM grain centroids that were also collected at load 0. The alignment between these datasets was accomplished through the use of the MJT MATLAB library [25], which registered the grain centroids between the datasets, using crystallographic misorientation between nf-HEDM and ff-HEDM grain orientations as a metric for that alignment. The nf-HEDM data consists of 69 grains fully contained in the center of the nf-HEDM volume (nf-volume 200 μm × 1 mm × 1 mm). These grains represent a subset of the nf-HEDM data but were selected as they each had a match to one of the grains in the ff-HEDM data. We found that these nf-HEDM grains registered within an average of 16.3 μm to a corresponding ff-HEDM grain centroid, and those matches had a mean misorientation of 0.13° between the ff-HEDM and the nf-HEDM grains. The specifics of the alignment procedure will be the focus of a future publication on the technique for registering large 3D datasets.

The nf-HEDM data collected at load 0 consists of five fields inside the HDF5 file: *Confidence Index*, *Grain ID*, *Location*, *Quaternions*, and *nNFpoints*. The number of individually measured nf-HEDM datapoints is contained in *nNFpoints*, while the spatial location of each datapoint (in Cartesian *x-y-z* notation) is contained in *Location*, and the crystallographic orientation of each datapoint, written as quaternions, is contained in the Quaternions field. In addition, each nf-HEDM datapoint is provided a grain assignment in the IceNine software, represented by an integer value, and recorded in the Grain ID field. After registering the datasets, the Grain ID in the nf-HEDM data corresponds exactly to the Grain ID in the ff-HEDM data. Multiple datapoints will belong to the same grain, which when assembled provides the morphology of the grain to within the resolution of the measurements (approximately 2 μm for this dataset). Finally, the confidence index, calculated based on the certainty that the orientation of the underlying nf-HEDM datapoint matches the diffraction pattern on the near-field detector [9], is provided in the Confidence Index field. This is a floating point number scaled between 0.0 and 1.0, where 1.0 means that 100 % of the simulated Bragg peaks from that pixel matched experimentally observed scattering. A greater degree of such overlap in the forward model technique provides greater assurance that the orientation in Quaternions is correct.

To view the data, a finite element mesh is included in the HDF5 datafile, contained in the *FEM* data field. Inside the FEM folder are the following fields: *connectivity*, *nelem*, *nnodes*, and *node*. The nelem and the nnodes fields are the number of elements (1.5 million) and the number of nodes (1,540,351), respectively, for this particular finite element mesh. The mesh consists of 8-node hexahedral finite elements. The node field contains the Cartesian location of the nodal points, while the connectivity field denotes how those nodes are assembled into a finite element mesh.

Fig. 3 The ff-HEDM data viewed on the accompanying finite element mesh. *Color* represents a grain identification number
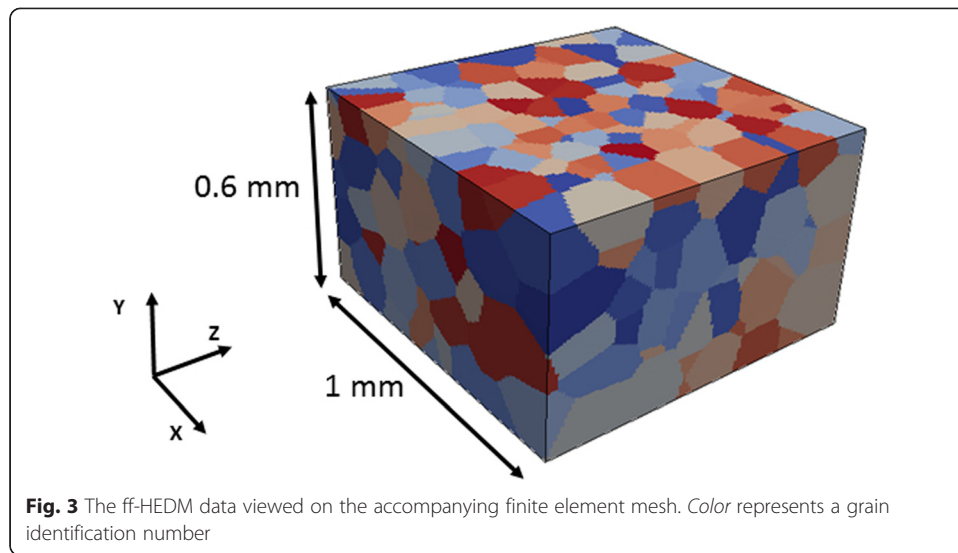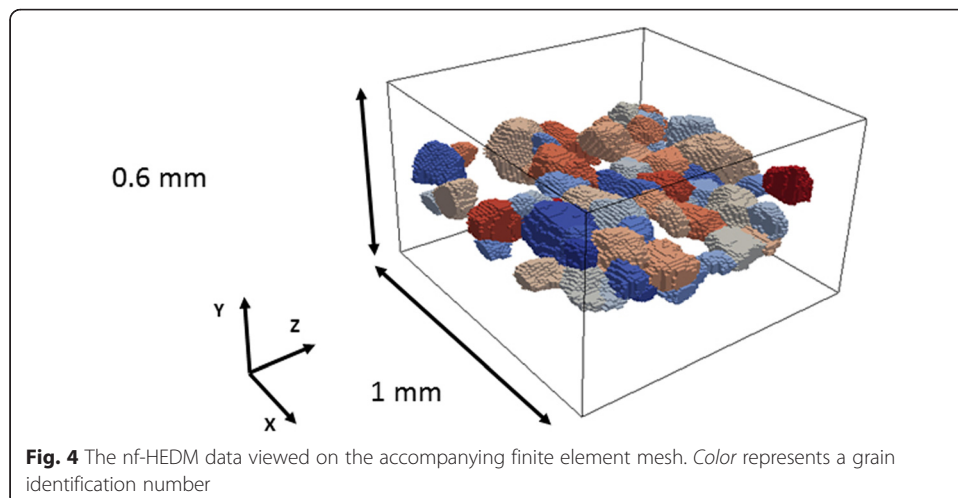
Figure 3 uses the finite element mesh as a means to view the ff-HEDM dataset. In this case, each element in the mesh is assigned a unique ff-HEDM grain, and multiple elements are assembled to represent the grains. The grains are then a voxellated representation of the actual grain, where in this case no distortion has been introduced to smooth the grain boundaries. The color of each grain represents the *Grain ID* field in the ff-HEDM data. Since only the ff-HEDM data are used in this representation, the exact morphology of the grains is not available as the element-to-grain assignment is similar to a 3D Voronoi representation of the grain structure, differing due to the voxellated nature of the elements. As the mesh density trends to infinity, the representation would converge toward an exact Voronoi representation.

Figure 4 uses the same finite element mesh to show the 69 grains used to align the nf-HEDM data with the ff-HEDM data. In this case, the morphology of the grains is

Fig. 4 The nf-HEDM data viewed on the accompanying finite element mesh. *Color* represents a grain identification number

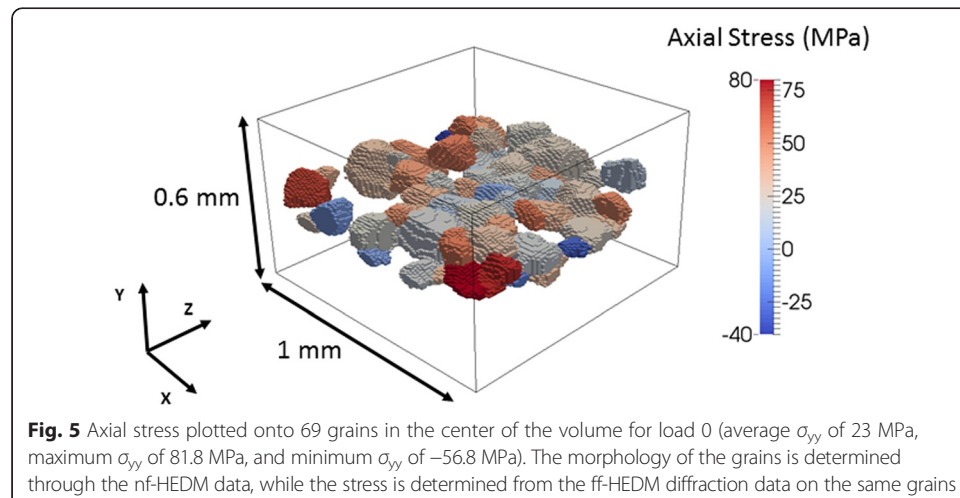Turner *et al. Integrating Materials and Manufacturing Innovation*

Page 7 of 9

represented to within the resolution of the finite element mesh. This shows the distinct difference in grain shape when using the full field morphology from the nf-HEDM data.
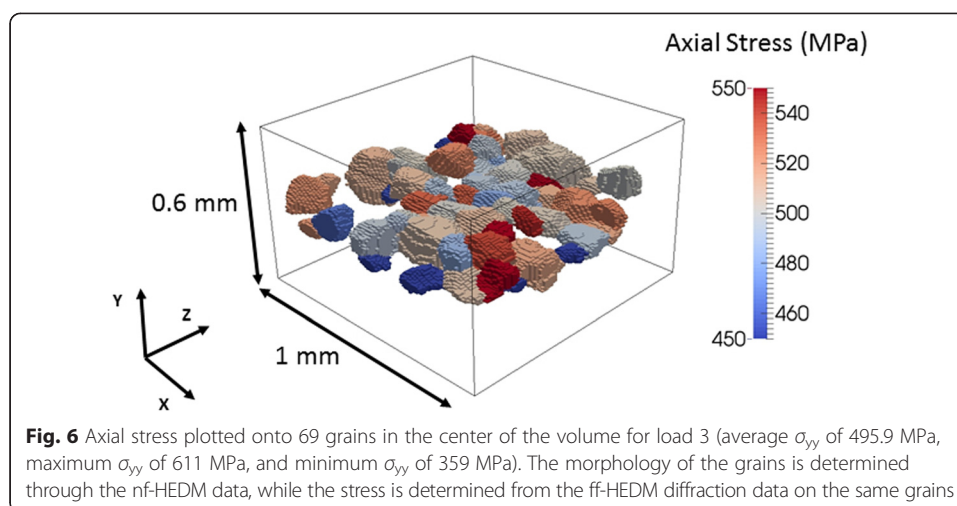
Potential applications of this dataset

The data discussed in this paper is a novel, first of its kind HEDM dataset that combines two distinct techniques with disparate data streams into a rich dataset for use in micromechanical model validation. For instance, Fig. 5 displays the axial stress component (σ_{yy}) determined from the ff-HEDM data for load 0 (nominally 23 MPa axial stress), plotted onto the nf-HEDM grains. This kind of data can be used to instantiate a CPFEM or other micromechanical modeling techniques such as the fast Fourier transform (FFT) methods. While the full aspects of these methods are beyond the scope of this work, many studies have directly incorporated microstructure into a micromechanical modeling framework and then attempted to validate the accuracy of the model on the microstructural level [26–34].

It is interesting to note from Fig. 5 that even with the processing schedule used in this work to minimize the residual stress in the material, significant grain-to-grain variation exists in the nominally unloaded state. The mean grain axial stress ranges from a minimum of −56.8 MPa to a maximum of 81.8 MPa. Some of this variation is undoubtedly due to the fact that load 0 is not truly an unloaded state, but the fact that some grains experience axial compression shows that any modeling technique would have to capture the initial grain-level stress variation to adequately capture the grain-level deformation in subsequent time-steps.

Figure 6 represents the analog to Fig. 5 but at the load 3 state (average axial stress of 495.5 MPa). Significant grain-to-grain variation in the axial stress component is still seen at this relatively high macroscopic load level. This kind of data can be directly compared to micromechanical models in order to validate the modeling methodology. This would allow an analysis of the accuracy of a given model, allowing the researcher the ability to change model parameters or formulation in order to better capture the deformation behavior at the microstructural level. In turn, this kind of data will then drive the development and use of models that incorporate a rich description of

Fig. 5 Axial stress plotted onto 69 grains in the center of the volume for load 0 (average σ_{yy} of 23 MPa, maximum σ_{yy} of 81.8 MPa, and minimum σ_{yy} of −56.8 MPa). The morphology of the grains is determined through the nf-HEDM data, while the stress is determined from the ff-HEDM diffraction data on the same grains

Turner *et al. Integrating Materials and Manufacturing Innovation*

Page 8 of 9

Fig. 6 Axial stress plotted onto 69 grains in the center of the volume for load 3 (average σ_{yy} of 495.9 MPa, maximum σ_{yy} of 611 MPa, and minimum σ_{yy} of 359 MPa). The morphology of the grains is determined through the nf-HEDM data, while the stress is determined from the ff-HEDM diffraction data on the same grains

microstructure, potentially enhancing engineering design by including more of the physics of materials science into the development of engineering components.

Availability and requirements of software used

Several software packages were used in the creation of this dataset. The HEXRD software package reduces the ff-HEDM diffraction data from the diffraction patterns on the area detector into the grain data presented in the HDF5 file. HEXRD is freely available for download and can be found on GitHub (https://github.com/praxes/hexrd). It was developed and tested under Linux Operating Systems. IceNine is another software package that analyzes the nf-HEDM data, reducing the data from the initial diffraction patterns to the point data found in the HDF5 file. It was also developed and tested under Linux Operating Systems, available on GitHub (https://github.com/FrankieLi/IceNine). MJT is a MATLAB library developed and maintained by the Air Force Research Laboratory. We developed this suite of library functions to further analyze the data from HEXRD and IceNine, registering the two datasets into a combined datafile found in the HDF5 file. MJT is available upon request and subsequent clearance of public release. It can run on any operating system running Matlab. However, the data presented in the HDF5 file format represent processed data that do not require the use of any of these software packages.

Availability of supporting data

The dataset supporting the results of this article is available in the NIST repository (http://hdl.handle.net/11256/599).

Endnotes

[1]Normally, this is referred to as residual stress. However, stress is an inferred quantity, as it cannot be directly measured. Rather, elastic strain is measured and converted to stress through the judicious use of a constitutive relationship.

Turner *et al. Integrating Materials and Manufacturing Innovation*

Page 9 of 9

Authors' contributions
TT and PS conceived the idea for the manuscript, and TT compiled the dataset and wrote the paper. PS, JB, SL, JS, JL, UL, PK, RS, BB, and JA collected the dataset. TT was not present at the data collection as he was deployed to Afghanistan and fighting the Taliban. JA is in charge of the 1-ID beamline of APS, and PK works there as a staff scientist. JB, SL, and JL conducted the extensive data reduction of the raw diffraction images, which were then further processed by TT for this paper. RS is one of the originators of the near-field technique and provided guidance throughout the process. BB built the phenomenal experimental test equipment that was pivotal to the data collection in this effort. All authors read and approved the final manuscript.

Author details
[1]Materials and Manufacturing Directorate, Air Force Research Laboratory, 2230 10th Street, Wright-Patterson AFB, OH 45433, USA. [2]Engineering Directorate, Lawrence Livermore National Laboratory, 7000 East Ave, Livermore, CA 94550, USA. [3]Carnegie Mellon University, 5000 Forbes Avenue, Pittsburgh, PA 15213, USA. [4]Deutsches Elektronen-Synchrotron, DESY-Petra III Notkestr. 85, 22603 Hamburg, Germany. [5]Advanced Photon Source, Argonne National Laboratory, 9700 S. Cass Ave, Argonne, IL 60439, USA. [6]PulseRay, 4583 State Route 414, Beaver Dams, NY 14812, USA.

References
1. Schuren JC, Shade PA, Bernier JV, Li SF, Blank B, Lind J, Kenesei P, Lienert U, Suter RM, Turner TJ, Dimiduk DM, Almer J (2015) Curr Opin Solid State Mater Sci 19:235
2. Lienert U, Li SF, Hefferan CM, Lind J, Suter RM, Bernier JV, Barton NR, Brandes MC, Mills MJ, Miller MP, Jakobsen B, Pantleon W (2011) JOM 63(7):70
3. Poulsen HF (2012) J Appl Crystallogr 45:1084
4. Dawson PR (2000) Int J Solids Struct 37:115
5. Turner TJ, Semiatin SL (2011) Model Simul Mater Sci Eng 19:065010
6. Turner TJ, Shade PA, Groeber MA, Schuren JC (2013) Model Simul Mater Sci Eng 21:015002
7. Poulsen HF (2004) Three-dimensional X-ray diffraction microscopy: mapping polycrystals and their dynamics. Springer, Berlin
8. Suter RM, Hennessy D, Xiao C, Lienert U (2006) Rev Sci Instrum 77:123905
9. Li SF, Suter RM (2013) J Appl Crystallogr 46:512
10. Poulsen HF, Nielsen SF, Lauridsen EM, Schmidt S, Suter RM, Lienert U, Margulies L, Lorentzen T, Jensen DJ (2001) J Appl Crystallogr 34:751
11. Margulies L, Lorentzen T, Poulsen HF, Leffers T (2002) Acta Mater 50:1771
12. Oddershede J, Schmidt S, Poulsen HF, Sorensen HO, Wright J, Reimers W (2010) J Appl Crystallogr 43:539
13. Bernier JV, Barton NR, Lienert U, Miller MP (2011) J Strain Anal Eng Des 46:527
14. Shade PA, Blank B, Schuren JC, Turner TJ, Kenesei P, Goetze K, Suter RM, Bernier JV, Li SF, Lind J, Lienert U, Almer J (2015) Rev Sci Instrum 86:093902
15. Lienert U, Brandes MC, Bernier JV, Weiss J, Shastri SD, Mills MJ, Miller MP (2009) Mater Sci Eng A 524:46
16. Brandes MC, Mills MJ, Williams JC (2010) Metall Mater Trans A 41:3463
17. Kwon J, Brandes MC, Sudharshan Phani P, Pilchak AP, Gao YF, George EP, Pharr GM, Mills MJ (2013) Acta Mater 61:4743
18. Pilchak AL (2013) Scripta Mater 68:277
19. Dawson P, Boyce D, MacEwen S, Rogge R (2000) Metall Mater Trans A 31:1543
20. Shade PA, Menasche DB, Bernier JV, Kenesei P, Park JS, Suter RM, Schuren JC, Turner TJ (2016) Fiducial marker application method for in situ multimodal x-ray experiments. J Appl Crystallogr 49. DOI:10.1107/S1600576716001989.
21. Hosford WF (1993) The mechanics of crystals and textured polycrystals. Oxford University Press, New York–Oxford
22. Tromans D (2011) IJRRAS 6(4)
23. Fisher ES, Renkin CJ (1964) Phys Rev 135:482
24. Frank FC (1991) Orientation Mapping. Metallurgical Transactions 19A:403
25. MJT MATLAB library developed by AFRL, available upon request with lead author @ Todd.Turner.5@us.af.mil
26. Turner T, Miller M (2007) J Eng Mater Technol 129:367–379
27. Dawson P, Boyce D, MacEwen S, Rogge R (2001) Mat Sci Eng A A313:123–144
28. Becker R, Panchanadeeswaran S (1995) Acta Metal Mater 43(7):2701–2719
29. Bhattacharyya A, El-Danaf E, Kalidindi SR, Doherty RD (2001) Int J Plast 17:861–883
30. Roters F, Eisenlohr P, Hantcherli L, Tjahjanto D, Bieler T, Raabe D (2010) Acta Mater 58:1152–1211
31. Zhao Z, Ramesh M, Raabe D, Cuitino A, Radovitzky R (2008) Int J Plast 24:2278–2297
32. Cedat D, Fandeur O, Rey C, Raabe D (2012) Acta Mater 60:1623–1632
33. Demir E, Raabe D, Zaafarani N, Zaefferer S (2009) Acta Mater 57:559–569
34. Lebensohn RA, Liu Y, Ponte Castaneda P (2004) Acta Mater 52:5347–5361